Linear and nonlinear microwave dynamics of vortices in $YBa_2Cu_3O_{7-\delta}$ thin films

N. Belk*
Department of Physics, Massachusetts Institute of Technology, Cambridge, Massachusetts 02139-4307; Lincoln Laboratory, Massachusetts Institute of Technology, Lexington, Massachusetts 02173-9108; and Rome Laboratory, Hanscom Air Force Base, Bedford, Massachusetts 01731-3010

D. E. Oates
Lincoln Laboratory, Massachusetts Institute of Technology, Lexington, Massachusetts 02173-9108 and Department of Physics, Massachusetts Institute of Technology, Cambridge, Massachusetts 02139-4307

D. A. Feld
Lincoln Laboratory, Massachusetts Institute of Technology, Lexington, Massachusetts 02173-9108

G. Dresselhaus
Francis Bitter Magnet Laboratory, Massachusetts Institute of Technology, Cambridge, Massachusetts 02139-4307 and Rome Laboratory, Hanscom Air Force Base, Bedford, Massachusetts 01731-3010

M. S. Dresselhaus
Department of Electrical Engineering and Computer Science and Department of Physics, Massachusetts Institute of Technology, Cambridge, Massachusetts 02139-4307

(Received 17 December 1996)

We report the results of a study of the nonlinear microwave surface impedance Z_s, i.e., its dependence on microwave current $Z_s(I_{\rm rf})$, resulting from vortex motion in $YBa_2Cu_3O_{7-\delta}$ thin films in a dc magnetic field applied parallel to the film's c axis. Using the technique of stripline resonators we have measured the nonlinear Z_s at frequencies of 1.23–8.45 GHz, at temperatures from 5 to 30 K, and in magnetic fields from 0 to 4 T. In the mixed state, there is a significant increase in R_s from the zero-field value, particularly at lower frequencies, causing an $R_s \propto f^{1.2}$ dependence at all measured temperatures and microwave powers. We also review our previously reported measurements and modeling of the linear Z_s because the nonlinear results can be explained by an extension of the model that we have previously used to describe the dependence of Z_s on frequency, temperature, and magnetic field in the linear $I_{\rm rf}$ regime. This model explains the linear Z_s data through the thermal activation of vortex segments between metastable vortex states separated by distances of order of the coherence length $\sim \xi$ and by a distribution of energy barriers U_b whose magnitudes extend from $U_b \sim 0$ K to at least several hundred K. We further show that the behavior of Z_s at high microwave powers is fully consistent with the same thermal activation of vortex segments, but the effective magnitudes of the energy barriers $\widetilde{U}_b$ have been reduced in proportion to the microwave current density $J_{\rm rf}(r,t)$ such that $\widetilde{U}_b = U_b - J_{\rm rf(}r,t)\,\phi_0 \xi l$. [S0163-1829(97)03142-1]

I. INTRODUCTION

Since the discovery of high-temperature superconductivity, it has been clear that understanding the behavior of high-T_c materials in a magnetic field would present a considerable challenge. They have been probed experimentally through a number of techniques such as torsional oscillators,[1] low-frequency ac magnetic permeability,[2,3] and microwave measurements of the complex surface impedance at both low[4–8] and high[7] microwave power levels.

Our use of stripline resonators[8–11] allows us to measure both the real part R_s and the imaginary part X_s of the microwave surface impedance Z_s of high-quality epitaxial thin films of $YBa_2Cu_3O_{7-x}$ (YBCO) at frequencies from 1.2 to 26 GHz. The Z_s depends critically on both the amplitude and phase of the vortex motion with respect to the applied rf field $H_{\rm rf}$.

We present here the results of an investigation of the linear and nonlinear microwave Z_s of YBCO in the mixed state in magnetic fields from 0 to 4 T, applied parallel to the c axis from 5 to 30 K and frequencies from 1.23 to 8.5 GHz. In this paper the nonlinear Z_s is denoted by $Z_s(I_{\rm rf})$ and is defined as the surface impedance that is dependent on microwave current. The linear surface impedance refers to the regime where Z_s is independent of the microwave current.

Our prior results in the linear regime show that the application of an external magnetic field causes R_s to increase significantly, particularly at low frequencies.[8] Further, as previously reported by us[7] and others,[12] we find that Z_s is proportional to the magnetic field, indicating that we are not probing collective effects,[13,14] but rather the interactions of individual vortices with defects in the YBCO, and that the length scales of these interactions are probably on the order of the coherence length $\xi \approx 20$ Å.[3,15–17] In the low-current linear-response data, the change in R_s due to the external magnetic field, ΔR_s, is proportional to T at low temperatures

TABLE I. Parameters of the films determined from both dc (four-point measurements) and microwave measurements. The penetration depth at $T=0$ K and in zero applied dc magnetic field $\lambda(0)$ is the parameter of a two-fluid model fit to our experimental points.

	dc Properties		rf Properties							
Film	d μm	Tc $(R=0)$	ΔR_{s0} $\Omega/(T$ GHz)	ΔR_{s1} $\Omega/(T$ K GHz)	$\alpha_P(0)$[a] N/m^2	f_1 (GHz)	r_{pl} nm^2	$U_{\delta 0}$ K	R_s $(T=5$ K) Ω	$\lambda(0)$ Å
1	0.24	91	1.22×10^{-6}	3.3×10^{-6}	3.6×10^{5}	1.23	19		2.5×10^{-5}	2650
2	0.58	89	4.7×10^{-7}	7.6×10^{-7}	9.7×10^{5}	1.47	12	$\sim 2U_b$	1.2×10^{-5}	2340
3	0.37	90.2	8.0×10^{-7}	4.2×10^{-7}	2×10^{5}	1.69	26	$2U_b+40$ K	1.8×10^{-5}	1600

[a]Extrapolated to $T=0$ K.

and proportional to $f^{1.2}$ at all fields and temperatures.[8]

We explained the T and f dependence of ΔR_s with a random vortex pinning potential. While the majority of the vortices is strongly pinned, with $\Delta R_s \propto f^2$ (Ref. 18) some are pinned in metastable states separated by energy barriers U_b.[19] Moreover, the dominant energy dissipation results from the transitions of vortex segments of length l between these metastable states that are formed by the pinning of the vortex cores by a random distribution of defects of volume $<\xi^3$ in the YBCO samples.[3,15–17] Because these pinning centers are small in volume, the range of the pinning interactions r_P is roughly equal to the vortex core size ξ, so that displacements of $\sim\xi$ can move a segment of a vortex core to a new pinning energy minimum. The random distribution of these defects results in a large number of closely spaced energy minima, separated by a random distribution of energy barriers with magnitudes extending down to ≈ 0 K. This gives rise to a broad distribution of characteristic frequencies for the hopping of vortex segments between metastable states and explains the frequency, temperature, and dc-magnetic-field dependences of ΔR_s and of the corresponding ΔX_s that are exhibited in our low-power linear-response data published earlier.[8] We show here that the same model also explains the high-power nonlinear response. Earlier measurements[7] have shown that the onset of nonlinearity, which is generally attributed to the current-induced depinning of vortices, occurs in these samples at current densities where typical vortex displacements are much less than the pinning range $\sim\xi$. While this apparent contradiction cannot be explained by the theories of vortex dynamics that assume relatively deep and uniform vortex pinning potentials,[20–22] we will show that the broad distribution of energy barriers between metastable vortex states, that can explain the frequency and temperature dependence of Z_s in the linear regime, can also explain the high-power nonlinear Z_s. In this work we concentrate on the temperature range $T \lesssim T_c/2$, where the temperature dependences of materials parameters, such as the mean distance between metastable states $r_P(T)$, the mean length of the metastable vortex segments $l(T)$, and the magnitudes of the energy barriers $U_b(T)$, are weak.

In the following, we present a description of our experimental techniques, specifically the manner in which we measure the surface impedance Z_s of our YBCO films. We then describe the details of the theory that we propose for fitting both the linear and nonlinear measurements that we have made. Finally, we discuss the results of those fits in the context of other work on vortex dynamics.

We introduce some notation conventions which we use throughout the paper in order to clarify the differences between dependences on dc magnetic field H and on microwave current $I_{\rm rf}$. The change to the *linear* Z_s due to the magnetic field is defined as $\Delta Z_s \equiv Z_s(H)-Z_s(H=0)$. The corresponding convention is used for ΔR_s and ΔX_s. The *nonlinear* $Z_s(I_{\rm rf})$ at constant magnetic field is defined as $\Delta_H Z_s \equiv Z_s(I_{\rm rf},H)-Z_s(0,H)$. The corresponding convention is used for $\Delta_H R_s$ and $\Delta_H X_s$.

II. EXPERIMENTAL METHODS

The microwave surface-impedance data were obtained in a liquid-He cryostat fitted with a 9-T superconducting magnet operating in a persistent current mode to ensure field stability. The samples were zero-field cooled to eliminate the possibility of trapped flux. The data presented were obtained at fields much greater than the lower critical field $H_{c1}\sim 0.01$ T to assure uniform penetration of our microwave resonators by the external field, as was verified through the use of a Hall-effect sensor.[7]

The samples were mounted in gold-plated copper or aluminum packages which were fixed to a carbon-glass thermometer, and mounted in a copper enclosure, which had a heater attached to its base. The temperature was monitored and controlled to obtain temperature stabilities of a few parts in 10^4.

The surface-resistance and -reactance data were obtained from YBCO samples grown on 0.5-mm-thick $LaAlO_3$ substrates. The samples were grown by different techniques. Samples 1 and 3 were 2500-Å and 3690-Å thick, respectively, and were produced through off-axis magnetron sputtering.[23,24] Sample 2 was 5800-Å thick, and was produced through cylindrical magnetron sputtering.[25,26] The properties of these films are listed in Table I. The three samples are high-quality epitaxial single-phase films with the c-axis perpendicular to the substrate.

The microwave properties were studied through the use of stripline resonators,[9,10] which are especially useful for measurements of the frequency and rf-current dependence of the surface impedance. These devices support standing waves whose microwave current has the form $I_{\rm rf}=I_0\sin(n\pi z/s)$ where n is the mode number and z is the position along the length s of the resonator. The resonant frequency for the modes is $f_n=nf_1$, where f_1 is the lowest frequency mode, which ranges from 1.2 to 1.7 GHz. The measurements were performed using a vector network analyzer and a series of

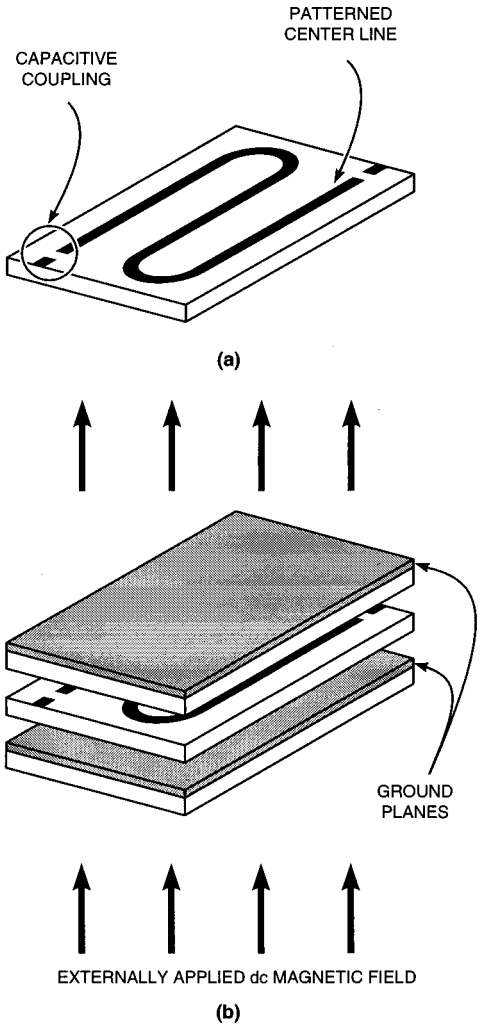

FIG. 1. View of the structure of a stripline resonator. (a) Patterned resonator line. The rf current flows in the plane parallel to the resonator line. (b) View of the resonator plus ground planes which form the top and bottom of the resonator cavity. The dc magnetic field is perpendicular to the plane of the film and parallel to the c axis of the YBCO.

broadband power amplifiers. This allowed measurements of mode frequencies from 1 to 26 GHz. To prevent radiation losses, the resonators were sandwiched between two superconducting ground planes which formed the top and bottom of a microwave cavity (stripline geometry). The sides of the cavity were formed by a gold-plated copper package in which the resonator and ground planes were mounted. The resonator, ground planes, and orientation of the applied field are shown in Fig. 1. At most measurement frequencies, the dynamics of the stripline completely dominate those of the surrounding cavity. However, some of the modes of the resonator are at frequencies very close to the modes of the cavity, and the resulting strong coupling makes them unsuitable for these experiments. Any residual cavity interactions with the remaining modes were minimized by considering only ΔZ_s, which is obtained by subtracting the zero-dc-field Z_s from the in-field Z_s at each frequency.

The striplines were weakly coupled so the measured Q was equal to the unloaded Q. Stripline widths were selected so that at the frequency f_1 each resonator had a zero-field low-temperature Q of about 10^5.

The microwave losses in the $LaAlO_3$ substrates, defined in terms of a loss tangent, produce a change in the resonator Q given by $1/Q_m = 1/Q + \tan\delta$, where Q_m is the measured quality factor and $\tan\delta \approx 2\times10^{-6}$ at low temperatures. This correction is small enough so that it is not significant in this work.[7,9] The shifts in resonant frequencies due to the changes in the Q of the resonator are of order $1/Q^2$ and are always negligible in comparison to the shifts we measure due to the changes in the sample's reactance.

As we discuss below, Z_s is determined by the complex microwave penetration depth $\tilde{\lambda}$ in these films. The real part of the zero-field microwave penetration depth $\tilde{\lambda}_R(H=0)$ is essentially equal to the London penetration depth λ_L at these frequencies. The imaginary part $\tilde{\lambda}_I(H=0)$ is proportional to $R_s(H=0)$. We extract $\tilde{\lambda}_R$ from measurements of the mode frequencies, determined by the stripline inductance L that is the sum of a geometrical component L_g and a kinetic component L_k that depends on $\tilde{\lambda}_R$ and on film thickness d. To obtain $L(\tilde{\lambda}_R)$ and the current density as a function of position in the resonator $J(\vec{r})$, we have used the results of Sheen *et al.*[10] Shifts in the surface reactance $\delta X_s(H,f,T,J_{\rm rf})$ due to any external variable such as H, f, T, or $J_{\rm rf}$ are determined from the measured shifts in mode frequencies δf_n by

$$\delta X_s(H,f,T,J_{\rm rf}) = 2\pi\mu_0 f\,\delta\tilde{\lambda}_R = -4\pi\mu_0 L\left(\frac{L}{L_{n0}}\right)^{1/2}\left[\frac{d}{d\tilde{\lambda}_R}L(\tilde{\lambda}_R)\right]^{-1}\delta f_n, \tag{1}$$

where f_{n0} and L_{n0} are, respectively, the zero-temperature, zero-field frequency, and inductance of a resonant mode n. Because $\delta\tilde{\lambda}_R$ is proportional to δf_n, and $\delta X_s = 2\pi\mu_0 f\,\delta\tilde{\lambda}_R$, we will generally quote the results for the shifts in X_s in the presentation of the data.

We obtain $\tilde{\lambda}_R(T=0,H=0)$ and the zero-field transition temperature T_c by incorporating the expression for the penetration depth taken from the two-fluid model[9,27]

$$\tilde{\lambda}_R(T) = \frac{\tilde{\lambda}_R(0)}{[1-(T/T_c)^4]^{1/2}} \tag{2}$$

into $L(\tilde{\lambda}_R)$ in Eq. (1) to obtain the frequency shift δf_n for a given mode as a function of T. The parameters $\tilde{\lambda}_R(0)$ and T_c are determined by fitting the mode frequency versus temperature data for the first mode.

The surface resistance R_s, which is proportional to $\tilde{\lambda}_I$, was extracted from the Q and f_n using the relationship:[10]

$$R_s = \frac{g(\tilde{\lambda}_R/d)f_n}{Q}, \tag{3}$$

where $g(\tilde{\lambda}_R/d)$ is a numerically determined function which accounts for the finite ratio of the film thickness d to $\tilde{\lambda}_R$.[9,10] The function $g(\tilde{\lambda}_R/d)$ also takes into account the stripline geometry, the characteristic impedance of the stripline, and the current distribution $J(\vec{r})$ within the resonator.

By using $g(\tilde{\lambda}_R/d)$ and $L(\tilde{\lambda}_R)$ in Eqs. (1) and (3),[9,10] the R_s and $\tilde{\lambda}_R$ determined from our data yield Z_s for ac currents flowing in a semi-infinite half-plane:

$$Z_s = R_s + iX_s = 2\pi\mu_0 i f\tilde{\lambda}, \tag{4}$$

in which R_s is taken to have a positive value. In the present work there are changes to $\tilde{\lambda}_R$ which result from the current-driven depinning of vortices, but, as we will show, the overall changes in the penetration depth, as determined by the changes in the mode frequencies, are less than 20% of the in-field penetration depth. Further, for the samples discussed in detail, the condition $\tilde{\lambda}_R < d/2$ prevails, so that the Q for these samples is only weakly dependent on $\tilde{\lambda}_R$.[10] In all of these measurements, the magnetic fields generated by the rf currents in the resonator are less than 1% of the applied dc magnetic field, and, as shown previously,[7] the zero-field surface resistance at all measured resonator currents is less than the in-field R_s at comparable currents.

III. THEORY

In the following subsections, we present theoretical results for $\tilde{\lambda}$ arising from the motion of vortices resulting from a dc magnetic field normal to the plane of the film.

A. $\tilde{\lambda}(H)$ in the limit of stationary vortices

In the absence of vortex motion, the field and temperature dependence of the London penetration depth[7] λ_L is given approximately as

$$\lambda_L(H,T) \approx \frac{\lambda_L(0,T)}{\sqrt{1 - H/H_{c2}(T)}}. \tag{5}$$

We are not sensitive to the temperature dependence of the upper critical field, because $H_{c2} \approx 100\ T \gg H$ and is only weakly dependent on T for $T \ll T_c$.[12,28–30] We exclude the temperature and field dependence of λ_L from our determination of $\Delta X_s(I_{\rm rf})$ by considering only $\Delta_H X_s \equiv [\Delta X_s(I_{\rm rf}) - \Delta X_s(0)]$ at a given T, f, and H. This allows us to separate the temperature and field dependence of the ΔX_s due to the nonlinear motion of vortices from the temperature and field dependence arising from changes in $\lambda_L(H,T)$.

When we exclude the effects of vortex motion, the imaginary part of $\tilde{\lambda}$ resulting from normal-fluid losses in the two-fluid model[31] is given as

$$\tilde{\lambda}_I = \mathrm{Im}\left\{\frac{\lambda_L}{[1 + 2i(\lambda_L/\delta_{\rm nf})^2]^{1/2}}\right\} \approx \lambda_L\left[\left(\frac{\lambda_L}{\delta_{\rm nf}}\right)^2\right], \tag{6}$$

where $\delta_{\rm nf}$ is the skin depth of the normal fluid. In this frequency and temperature regime, $\delta_{\rm nf} \approx 3\ \mu$m. Since the measured $\delta_{\rm nf}$ are relatively small at low temperatures it is normally assumed that a significant density of unpaired electrons is present in extrinsic defects such as grain boundaries and weak links.[11] Because $\lambda_L/\delta_{\rm nf} \ll 1$ and because λ_L is a weak function of magnetic field, the effect of the normal fluid losses is almost completely contained in the zero-field surface resistance $R_s(0)$. Thus, by subtracting the zero-field $R_s(0)$ data from the in-field $R_s(H)$ data at each temperature and by focusing on $\Delta R_s(H) \equiv R_s(H) - R_s(0)$, we can isolate the losses associated with the motion of vortices. Furthermore, normal-fluid losses will contribute a $\Delta R_s \propto f^2$ frequency dependence which is very different from the $\Delta R_s(H) \sim f^{1.2}$ dependence we have measured in all samples and at all temperatures.[7,8]

B. $\Delta\tilde{\lambda}$ arising from vortex motion

In order to determine the contribution of the motion of vortices to Z_s, it is necessary to determine the electric field E they generate as a result of their displacements u. The electric field is proportional to their velocity $\dot{u}$ and is given by $E \propto \Sigma(\phi_0\dot{u})$ where ϕ_0 is the flux quantum and the sum is over all vortex segments. We have shown[8] that at $T \lesssim T_c/2$ and $f < 25$ GHz there are two principal types of vortex dynamics that contribute to the overall Z_s in high-T_c materials. The first is due to the majority of vortices which are pinned in parabolic wells and whose viscosity is sufficiently small that their displacements u_P are in phase with the applied microwave current at all measured frequencies.[8,20–22,32] The second type of vortex motion, described by the displacements u_h, arises from the thermally activated hopping of vortex segments between pairs of metastable vortex states.[8] In this section we outline the calculation of ΔZ_s arising from both kinds of motion.

1. Pinned vortex segments

For the first case, vortices pinned in parabolic wells, the u_P of the vortex segments, when driven by an rf current density $J_{\rm rf}(\vec{r},t) = J_{\rm rf}(\vec{r})e^{2\pi i f t}$ perpendicular to H, are determined by a force balance equation of the form:[20–22]

$$2\pi i f \eta u_P l + \alpha_P u_P l = J_{\rm rf}(\vec{r},t)\phi_0 l, \tag{7}$$

where l is the length of the pinned vortex segment, η is the linear vortex viscosity per unit length, and α_P is the vortex restoring force per unit length. It is customary to define the pinning frequency[8,12,29] by

$$f_P = \frac{\alpha_P}{2\pi\eta} \sim 10^{11}\ \text{Hz}, \tag{8}$$

which is the frequency at which the pinned vortex segments are no longer able to move fast enough to remain in phase with the applied microwave field.

The α_P is related to the vortex pinning potential energy $U(u)$ by the relation

$$\alpha_P \approx \frac{1}{l}\frac{\partial^2 U(u)}{\partial u^2}. \tag{9}$$

In what follows, as other authors have done,[19,20,22,33] we take l as the mean length and α_P as the mean vortex restoring force constant per unit length. Since our measurements indicate that ΔZ_s is proportional to the magnetic field,[7,8] we conclude that α_P is dominated by interactions between individual vortex cores and pinning centers in the YBCO samples rather than by vortex-vortex interactions. Inverting Eq. (7) and taking a time derivative of u_P gives the velocity of an individual pinned vortex segment in response to the microwave current density $J_{\rm rf}(\vec{r},t)$:

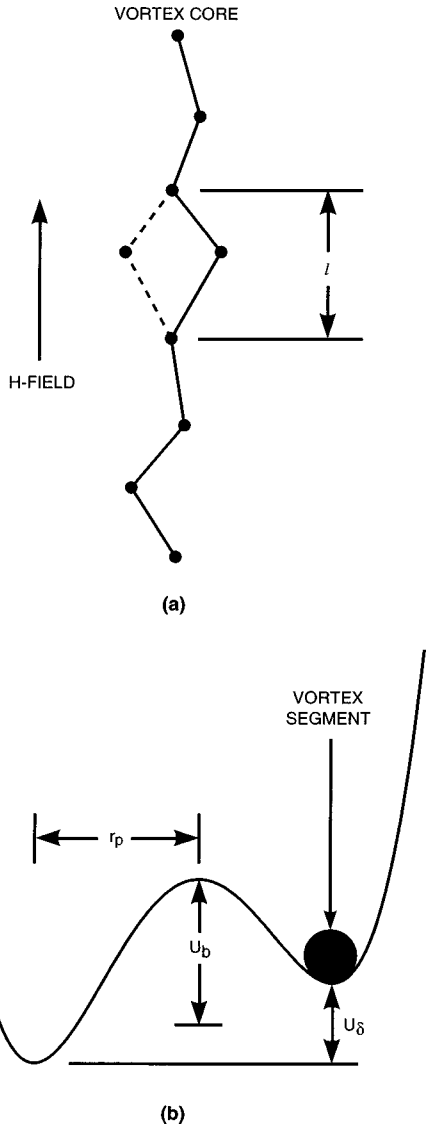

FIG. 2. (a) A metastable vortex segment of length l with two possible metastable pinning sites. (b) The effective pinning potential seen by the metastable segment and the parameters describing this pair of states: separation r_P, average barrier height U_b seen by the potential minima, energy difference U_δ between potential minima, and segment length l. The energies of the two potential minima are $U_b \pm U_\delta$.

$$\dot{u}_P = \frac{1}{\alpha_P}\frac{2\pi i f}{1+if/f_P} J_{\rm rf}(\vec{r},t)\,\phi_0, \tag{10}$$

where $f \ll f_P$ for the data presented here. We expect, for the $J_{\rm rf}$ levels studied in this work, that u_P will grow linearly with $J_{\rm rf}$. As a result, $\Delta Z_s(H) \propto \dot{u}/J_{\rm rf}$ will be independent of the current for the strongly pinned vortices.

2. Hopping vortex segments

The second type of vortex motion which contributes to ΔZ_s is the thermally activated hopping of vortex segments between pairs of metastable states. Because of the time required to overcome the barriers between these states, these vortices respond more slowly to $J_{\rm rf}$ and move distances $\sim 2r_P \sim 2\xi \approx 50$ Å. Figure 2 shows a metastable vortex segment of length l capable of moving between two states separated by an energy barrier whose average height seen from the two minima is U_b and having an energy difference U_δ. The number of these segments at $-r_P$ is proportional to $(u_h - r_P)$, and the number of segments at r_P is proportional to $(u_h + r_P)$. The mean velocity of the ensemble of vortex segments moving from an initial site at mean position $-r_P$, with respect to the barrier, to a final site at mean position $+r_P$ is determined by the probability of the vortex segment ensemble being found at $-r_P$ times the rate at which the segments are activated from $-r_P$ to $+r_P$, minus the probability that the vortex segment ensemble is at $+r_P$ multiplied by the rate at which the segments are activated from $+r_P$ to $-r_P$. The rate at which a vortex segment is activated from a state is determined by an attempt frequency f_a which we take to be $\approx f_P$ times the exponential of the instantaneous barrier height seen by the vortex segment in that state. Therefore, the velocity of a vortex segment hopping over an energy barrier between two metastable states separated by $2r_P$ driven by a microwave current density $J_{\rm rf}$ perpendicular to H is

$$\frac{\dot{u}_h}{\pi} = -(u_h + r_P) f_a \exp\left[\frac{-U_b - J_{\rm rf}(\vec{r},t)\,\phi_0 l r_P - U_\delta/2}{k_B T}\right] - (u_h - r_P) f_a \exp\left[\frac{-U_b + J_{\rm rf}(\vec{r},t)\,\phi_0 l r_P + U_\delta/2}{k_B T}\right]. \tag{11}$$

In Eq. (11) the exponentials determine the rates at which the vortex segments are activated over barriers of instantaneous heights $U_b \pm U_\delta \pm J_{\rm rf}(r,t)\,\phi_0 l r_P$. In what follows we define $f_{Th} = f_a \exp\{-U_b/k_B T\}$ so Eq. (11) can be simplified giving

$$\frac{\dot{u}_h}{2\pi f_{Th}} = -u_h \cosh\left[\frac{r_P l \phi_0 J_{\rm rf}(r,t) + U_\delta/2}{k_B T}\right] + r_P \sinh\left[\frac{r_P l \phi_0 J_{\rm rf}(r,t) + U_\delta/2}{k_B T}\right], \tag{12}$$

where $J_{\rm rf}(\vec{r},t) = J_{\rm rf}(\vec{r}) e^{2\pi i f t}$ and $J_{\rm rf}(\vec{r})$ is numerically determined as discussed in Sec. II.

We integrate $\dot{u}(U_b, U_\delta, \vec{r}) = \dot{u}_h + \dot{u}_P$ over the probability distributions $\nu(U_b)$ and $\nu(U_\delta)$, discussed below, to determine the mean time-averaged vortex velocity $\dot{u}(\vec{r})$ at each point in the resonator. This velocity is determined from Eqs. (10) and (12) by

$$\dot{u}(J_{\rm rf}, f, T) = f \int_{-\infty}^{\infty} dU_\delta \int_0^{\infty} dU_b \int_0^{1/f} dt\; \dot{u}(U_b, U_\delta) \times [\cos(2\pi f t) + i\,\sin(2\pi f t)]\,\nu(U_b)\,\nu(U_\delta). \tag{13}$$

3. Determination of $\nu(U_b)$ and $\nu(U_\delta)$ from $Z_s(T,f)$ in the linear limit

In order to use Eq. (13) to model the dynamics of vortices, it is necessary to find $\nu(U_b)$ and $\nu(U_\delta)$ from the measured linear response of the system. In the linear limit, where $J_{\rm rf}\phi_0 r_P l < k_B T$, Eq. (12) can be simplified to give

$$\dot{u}_h = \frac{r_P^2 l}{k_B T}\left(\frac{2\pi i f}{1+if/f_{Th}}\right) J_{\rm rf}(\vec{r},t)\,\phi_0, \tag{14}$$

which has the same form as Eq. (10), but, as we will discuss, the distribution of f_{Th} is very different from that of f_P. As a result ΔZ_s arising from the $\dot{u}_h$ behaves quite differently from that arising from the $\dot{u}_P$. At any temperature, the total ΔR_s resulting from vortex hopping in the small $J_{\rm rf}$ limit $\Delta R_s \propto \Re(\Sigma \dot{u}_h/J_{\rm rf})$ is proportional to the number of metastable segments for which $U_\delta < k_B T$ and for which $f_{Th} \sim f$. Assuming an approximately constant distribution of U_δ in the range $U_\delta < k_B T$, the number of states for which $U_\delta < k_B T$ is $\nu(U_\delta = 0) \times k_B T$, where $\nu(U_\delta)$ is the probability of finding two metastable states separated by a given energy U_δ. The number of metastable states which have a given f_{Th} in the span Δf_{Th} is proportional to the density of barrier heights $\nu[U_b = k_B T \ln(f_{Th}/f)]$ multiplied by the factor $(dU_b/df_{Th})\Delta f_{Th} = (-k_B T/f_{Th})\Delta f_{Th}$. Therefore, as we will discuss below, the overall sample $\Delta R_s(T,f) \propto \Re(\dot{u}/J_{\rm rf})$ is roughly proportional to $\dot{u}_h$ in Eq. (14) integrated over f_{Th} where the integrand is multiplied by the factor $\nu(U_\delta = 0)\,\nu[U_b = k_B T \ln(f_{Th}/f)]k_B T^2/f_{Th}$.[34]

As shown by Koshelev and Vinokur, the frequency dependence of $\Delta R_s(T,f)$ arising from vortex hopping in the linear regime[19] is always $\sim f^1$. To produce the $\Delta R_s(T,f) \propto T^1$ dependence that we find experimentally at low temperatures and low $I_{\rm rf}$ (Fig. 4), $\nu(U_b)$ must be roughly independent of both T and U_b.[19] However, the temperature dependence of $\Delta R_s(T,f)$ is influenced by the temperature dependences of r_P, l, U_b, and f_a, the energy dependence of $\nu(U_b)$, and in addition $\Delta R_s(T,f)$ may be affected by the quantum-mechanical properties of vortices at low temperatures.[33,35] Because there is no detailed understanding of the behaviors of these parameters, we do not attempt an exact explanation of the temperature dependence of ΔR_s, but rather we show that the behavior of the temperature dependence of the nonlinear $\Delta R_s(J_{\rm rf})$ is predicted from that of the linear ΔZ_s. The product of $\nu(U_b \sim 0)$ and $\nu(U_\delta \sim 0)$ is a fitting parameter that we obtain from our linear ΔR_s data by requiring the slope of $\Delta R_s(T)$ vs temperature to be equal to the measured slope of $\Delta R_s(T)$ arising from the hopping of vortices for each sample in the limit of zero current. In what follows we define this slope as ΔR_{s1} and in addition, because in the limit of zero temperature and zero current, $\Delta R_s(T)$ does not extrapolate to zero, we add a small temperature independent ΔR_{s0} to all of our numerically generated curves so that the small $I_{\rm rf}$ response of the measured ΔR_s is accurately reproduced. These fitting parameters are given in Table I for each of the samples.

4. ΔZ_s in the nonlinear limit

In the limit $J_{\rm rf}\phi_0 r_P l > k_B T$, the microwave current is able to drive vortices between metastable states with energies $U_b, U_\delta \gg k_B T$ so the allowed range of U_δ which contributes to Z_s becomes much greater than at small current. In order for a vortex segment to move between metastable states, $J_{\rm rf}(\vec{r})\phi_0 r_P l$ must be greater than roughly $U_b + |U_\delta/2| - k_B T \ln f_a/f$. Therefore, as $|U_\delta|$ increases, U_b decreases for vortex segments which are able to hop. As U_b decreases, the work done by $J_{\rm rf}$ in pushing vortex segments between metastable states decreases and therefore ΔR_s also decreases. As a result, in both the linear and nonlinear limits, ΔR_s is dominated by $\nu(U_\delta)$ at small U_δ.

In this model, ΔX_s is determined by the number of vortex segments which are able to hop, with only a weak dependence on $|U_\delta|$. Thus, for large $J_{\rm rf}$, in order to fit our nonlinear ΔX_s data, we need to determine the $\nu(U_\delta)$ for all U_δ. For large $J_{\rm rf}$ and energy independent $\nu(U_\delta)$ our numerical results show that $\Delta_H X_s \equiv \Delta X_s(I_{\rm rf}) - \Delta X_s(0)$ grows with $J_{\rm rf}$ at twice the rate of $\Delta_H R_s \equiv \Delta R_s(I_{\rm rf}) - \Delta R_s(0)$. This ratio of $\Delta_H X_s/\Delta_H R_s$ is larger than the ratio of ≈ 1.5 that we obtain from our measured data, indicating that the time-averaged energy difference between two metastable states U_δ does not become arbitrarily large in our samples. The U_δ can be constrained in two ways: the first is to assume that the energy minima of both metastable states tend to be lower than the energy maximum of the barrier between the states $(U_\delta < 2U_b)$, and the second is to assume that $\nu(U_\delta)$ is a decreasing function of energy for large U_δ. We have found that the simplest way to approximate our ΔX_s data is to introduce the parameter $U_{\delta 0}$ into our numerical solution of Eq. (13) so that $\nu(U_\delta) = 0$ when U_δ is greater than the empirically determined value $U_{\delta 0}$.

In order to determine Z_s from $\dot{u}$ we define the complex effective vortex resistivity $\rho_v = B\phi_0\dot{u}/J_{\rm rf}$ arising from the electric field generated by vortex motion $(E \propto \phi_0 \dot{u})$.[8,19,20] Since the current density over the sample is not uniform, it is necessary to do a spatial average over $J_{\rm rf}$ to obtain $\rho_v(I_{\rm rf},f,T)$ from $\rho_v(\vec{r},J_{\rm rf},f,T)$:

$$\rho_v(I_{\rm rf},f,T) = \frac{\int d^3 r J_{\rm rf}^2(\vec{r})\rho_v(J_{\rm rf}(\vec{r}),f,T)}{(\int d^3 r J_{\rm rf}(\vec{r}))^2}, \tag{15}$$

where $I_{\rm rf}$ is the total resonator current $\int d^2 r J_{\rm rf}(\vec{r})$ integrated over the cross-sectional area at the current maximum of the resonator standing wave.

The $\Delta_H Z_s$ is determined from λ_L and ρ_v by the following equation:[19–21]

$$\Delta_H Z_s = 2\pi\mu_0 i f \tilde{\lambda} = 2\pi\mu_0 i f\left[\lambda_L^2 + \frac{\rho_v(I_{\rm rf},f,T)}{2\pi i f \mu_0}\right]^{1/2}. \tag{16}$$

This is the usual expression for $\tilde{\lambda}$, but here we incorporate our derivation of $\rho_v(I_{\rm rf})$ arising from a strongly disordered pinning potential. It is this equation that, incorporating the results of Eqs. (10), (12), (13), and (15), is used to fit our measured data. In writing Eq. (16) we have neglected the effects of the normal fluid losses [Eq. (6)], but as discussed previously, these effects are removed from the results we present since we subtract the zero-field $Z_s(0)$ from the in-field $Z_s(H)$.

When $\Re[\rho_v/(2\pi i f \mu_0)] \ll \lambda_L^2$ a first-order expansion of Eq. (16) gives $\Delta_H Z_s \sim \rho_v$. Since $\rho_v \propto \dot{u}$, the harmonic motion of the vortices pinned in parabolic wells [Eq. (10)] will contribute a real part of $Z_s \propto f^2$ for $f \ll f_P$. As discussed previously, for $\nu(U_b)$ roughly independent of U_b, the quantity ΔR_s arising from the hopping of vortices will be proportional to $f^1 T^1$ at low $I_{\rm rf}$. Because the ΔR_s arising from the hopping of vortices is $\propto f^1$ and is $I_{\rm rf}$ dependent it is easy to separate it from the component of ΔR_s arising from strongly

pinned vortex for which ΔR_s is $I_{\rm rf}$ independent and $\propto f^2$. However, the two components of ΔX_s are more difficult to isolate.

The $\Delta X_s(T,H,I_{\rm rf})$ arising from the motion of vortices is determined by the mode frequency multiplied by the number of vortices which are able to move fast enough that they remain in phase with $I_{\rm rf}$. For $f \ll f_P \sim 10^{11}$ Hz, all of the pinned vortices [Eq. (10)] satisfy this condition, and for the hopping vortices there is only a weak frequency dependence of the number of vortices which contribute to ΔX_s. Therefore, both populations of vortices give $\Delta X_s \propto f^1$. Because, as shown previously,[8] ΔX_s is dominated by both the $I_{\rm rf}$-independent $\Delta X_s(T,H)$ of the pinned vortices for which $\dot{u}(T,H)$ is proportional to f [Eq. (10)], and the $I_{\rm rf}$-independent $\lambda_L(T,H)$ which also contributes a $\Delta X_s \propto f^1$ dependence [Eq. (16)], we isolate the rf current-dependent $\Delta X_s(T,H,I_{\rm rf})$, arising from the hopping of vortices, by presenting $\Delta_H X_s \equiv \Delta X_s(T,H,I_{\rm rf}) - \Delta X_s(T,H,0)$.

In the nonlinear limit, Eq. (16) predicts that a contribution to ΔR_s will result from the work done by $J_{\rm rf}$ as it pushes each active vortex segment over its barrier U_b. This will occur twice during each rf cycle so that the energy dissipated per unit time will be proportional to f, and therefore $\Delta_H R_s$ will still be proportional to f^1 in the nonlinear regime. The $\Delta_H R_s$ will tend to be determined by those vortices having larger U_b and U_δ values. Since increasing $J_{\rm rf}$ will linearly increase the mean values of the U_b and the range of the U_δ of the active metastable vortex segments, the energy dissipated by the metastable segments for which $J_{\rm rf}\phi_0 r_P l > U_b, U_\delta$ will grow quadratically in $J_{\rm rf}$. Therefore, the electric field $E \propto \dot{u}$ arising from the segments able to hop between metastable states increases as $J_{\rm rf}^2$, and the $\Delta_H R_s \propto E/J_{\rm rf}$ will increase like $I_{\rm rf}^1$ in the data. However, if $\nu(U_b)$ is roughly constant, the additional ΔR_s, arising from the effect of thermally activating vortex segments over the energy barriers, will be comparable at all $J_{\rm rf}$, causing the number of states within $k_B T$ of $U_b = J_{\rm rf}\phi_0 r_P l$ to be independent of $J_{\rm rf}$. As a result, in the measured data at high $I_{\rm rf}$, the dependence of $\Delta_H R_s$ on T, f, H, and $I_{\rm rf}$ is

$$\Delta_H R_s(T,f,H,I_{\rm rf}) \approx H f^1 [a I_{\rm rf} + \Delta R_{s0} + \Delta R_{s1} T^1], \quad (17)$$

where a is a constant and the H dependence applies as long as both H and $I_{\rm rf}$ are small enough so that the vortex system remains in the single vortex limit.[12,22]

In addition, $\Delta_H X_s(I_{\rm rf})/f$ is proportional to the component of the motion of the vortices which is in-phase with $J_{\rm rf}$; therefore, as $J_{\rm rf}$ is increased, the number of metastable segments for which $J_{\rm rf}\phi_0 r_P l > U_b, U_\delta$ will increase as $J_{\rm rf}^2$ so that $E \propto \dot{u}$ arising from the kinetic inductance of the vortices will grow like $J_{\rm rf}^2$, and $\Delta_H X_s$ will grow linearly with $I_{\rm rf}$. For large $J_{\rm rf}$, the states for which $J_{\rm rf}\phi_0 r_P l > U_b$ are U_δ polarizable at all measured values of f. As a result, in the nonlinear limit, the component of $\Delta_H X_s = \Delta X_s(I_{\rm rf}) - \Delta X_s(0) \propto E$ arising from the hopping of vortices is expected to grow linearly with frequency for $J_{\rm rf}\phi_0 r_P l \gg k_B T$. However, the magnitude of the contribution of the thermally activated vortices to $\Delta_H X_s$ is not expected to be changed appreciably as T increases. As a result, at high $I_{\rm rf}$, $\Delta_H X_s(T,f,H,I_{\rm rf})$ is given by

$$\Delta_H X_s(T,f,H,I_{\rm rf}) \approx H f^1 [a I_{\rm rf} + \Delta X_{sa}(T)], \quad (18)$$

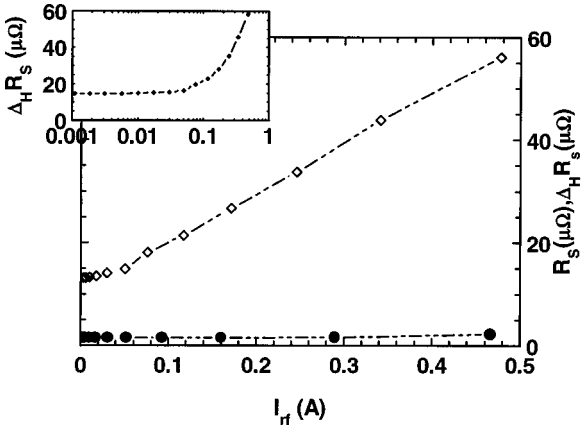

FIG. 3. The (◇) show $\Delta_H R_s$ vs current $I_{\rm rf}$ for sample 1 at $f = 1.23$ GHz and $T = 4.7$ K for $H = 1$ T. For reference the curve (●) $R_s(H = 0$ T) is shown. The inset shows $\Delta_H R_s$ vs $I_{\rm rf}$ on a logarithmic scale in order to show the behavior at low values of $I_{\rm rf}$ more clearly. The $\Delta_H R_s$ is nearly constant for $I_{\rm rf} < 0.03$ A.

where the temperature dependence $\Delta X_{sa}(T)$, which will be similar to that of $\Delta R_s(T)$, is obscured by the temperature dependence of $\Delta_H X_s(H,T)$ arising from the majority of vortices which are strongly pinned.

IV. EXPERIMENTAL RESULTS

Figure 3 shows $\Delta_H R_s$ at a field of 1 T and R_s in zero field for sample 1 as a function of $I_{\rm rf}$ for $f = 1.23$ GHz and $T = 4.7$ K, illustrating that $\Delta_H R_s$ at 1 T is more than an order of magnitude greater than the surface resistance at 0 T over the measured current range. In the inset, the $H = 1$ T data is shown on a logarithmic scale. The $\Delta_H R_s$ data at $H = 1$ T are only weakly dependent on $I_{\rm rf}$ for $I_{\rm rf} < 0.06$ A. For $I_{\rm rf} > 0.06$ A, $\Delta_H R_s$ grows with increasing $I_{\rm rf}$ and the sample is in the nonlinear regime. In order to determine the vortex displacements arising from an $I_{\rm rf}$ of 0.06 A, we have determined the vortex restoring force constant α_P from ΔX_s and Eqs. (10) and (16), for the three resonators discussed here (see Table I). As we have shown,[8] this is an underestimate, since we have ignored the contribution of vortex hopping to ΔX_s As a result, the actual α_P is 10–20% larger. The average vortex displacement u_P is approximately $J_{\rm rf}\phi_0/\alpha_P$, and a resonator current of 0.06 A corresponds to a maximum current density in the stripline resonator of only 1.8×10^6 A/cm^2. As a result, for a measured α_P of 3.6×10^5 N/m^2 (sample 1),[8] we determine vortex displacements of only 1.2 Å at $J_{\rm rf} = 1.8 \times 10^6$ A/cm^2 ($I_{\rm rf} = 0.06$ A).[7] As this group[7] and others[12] have found, the onset of nonlinearity is at vortex displacements much smaller than that $\xi \approx 20$ Å required to significantly change the vortex pinning force.[7,22] In the range from $I_{\rm rf} \approx 0.1$ to 0.5 A, Fig. 3 shows that $\Delta_H R_s(I_{\rm rf})$ changes by a factor of ≈ 4 and is $\propto I_{\rm rf}$. The low value of current density at which vortices can be depinned is explained by the existence of energy barriers between vortex states whose magnitudes extend to $< k_B T \ln(f_a/f_n)$. While the vast majority of vortices do not gain enough energy from $J_{\rm rf}$ to move to adjacent states at $J_{\rm rf} = 1.8 \times 10^6$ A/cm^2, there is a small number of vortex segments whose hopping probability is significantly increased

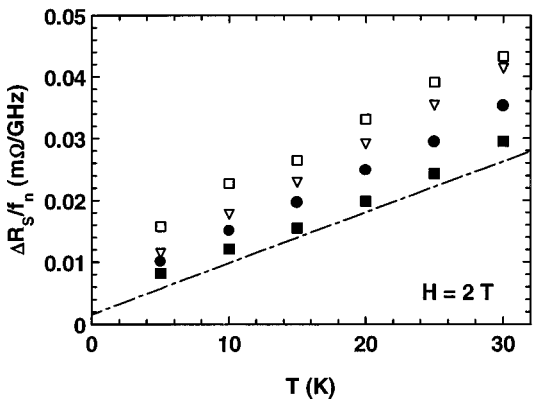

FIG. 4. The ΔR_s of sample 3 divided by $f_n^{1.0}$ at temperatures from 5 to 30 K at 5 K intervals for four different frequencies: (■) $f=1.69$ GHz, (●) $f=3.38$ GHz, (▽) $f=6.7$ GHz, (□) $f=8.45$ GHz. The dashed line, determined from these data, is of slope ΔR_{s1} and has an intercept of ΔR_{s0}.

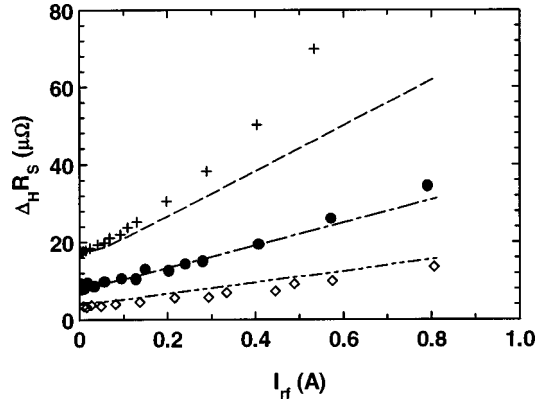

FIG. 5. Plot of $\Delta_H R_s$ vs current $I_{\rm rf}$ for sample 2 at $f=1.47$ GHz and $T=5.0$ K for three magnetic fields: (⊕) $H=1$ T, (●) $H=2$ T, and (+) $H=4$ T. The curves show the fits of Eq. (16) to the data.

by $J_{\rm rf}$, and these vortices contribute a nonlinear component to ΔR_s. In addition, the roughly 400% increase in $\Delta_H R_s$ that is $\propto I_{\rm rf}$ for rf currents between 0.06 and 0.5 A is consistent with the expected behavior of $\Delta_H R_s$ in the proposed model with $\nu(U_b)$ roughly independent of U_b. As $J_{\rm rf}$ is increased, the number of vortex segments for which $U_\delta < J_{\rm rf}\phi_0 r_P l$ increases linearly, as does the mean value of the U_b for the active states, so that the overall $\dot{u}$ and E are both proportional to $J_{\rm rf}^2$. Therefore $\Delta_H R_s \propto E/J_{\rm rf}$ is proportional to $I_{\rm rf}$.

In Fig. 4 we show the linear $\Delta R_s/f_n$ at 2 T of sample 3 vs temperature for several mode frequencies. Samples 1 and 2 show similar behavior, as discussed in detail in Ref. 8. The similarity of the slopes shows that $\Delta R_s = \Delta R_{s,Th} + \Delta R_{s,a}$ where $\Delta R_{s,Th} \propto f^1$ results from the activation of vortices between metastable states and $\Delta R_{s,a} \propto f^2$ results from strongly pinned vortices. The spreading in the curves probably arises from $\Delta R_{s,a}$ increasing slowly with temperature, but may reflect an error of 10–20% in the exponent 1.0 of the term due to vortex hopping. By linearly extrapolating the slopes of these data to $f=0$ we obtain an approximation for the slope of $\Delta R_s(T)$ arising from the hopping of vortices which we define as ΔR_{s1}. By extrapolating these data to $f=0$ and $T=0$ we find the zero-temperature intercept which we define as ΔR_{s0}. The dashed line shown in Fig. 4 is of slope ΔR_{s1} and the intercept is ΔR_{s0}. The values for ΔR_{s0} and ΔR_{s1} are listed in Table I for each sample and are used below to fit the sample data to the proposed model. The roughly $\Delta R_s \propto T$ dependence seen in the component of $\Delta R_s \propto f$ is consistent with the proposed model if $\nu(U_b)$ is independent of U_b for energies less than ~ 100 K as in sample 1 (see Fig. 3). As T is increased, both the number of vortex segments for which $U_\delta < k_B T$, and the range of the U_b for the active states increases linearly, so that the number of active states increases as T^2. However, due to thermal fluctuations, the polarizability of the states is $\propto 1/T$ [Eq. (12) and (14)] so that $\dot{u}_h$ and the electric field $E \propto \Delta R_s$ are both proportional to T.

Figure 5 shows the change in surface resistance $\Delta_H R_s$ of sample 2 as a function of the microwave current $I_{\rm rf}$ at fields of 1, 2, and 4 T for $f=1.47$ GHz and $T=5$ K. It can be seen that the $\Delta_H R_s$ at 2 T is roughly twice that at 1 T, indicating that ΔR_s at constant $I_{\rm rf}$ remains $\propto H$ even in the nonlinear region. This result extends to higher $I_{\rm rf}$ values the findings of various authors[7,8,13,32] who have found that the linear Z_s is $\propto H$ in high-T_c materials. At 4 T, however, $\Delta_H R_s(I_{\rm rf})$ increases faster than $I_{\rm rf}^1$ at high $I_{\rm rf}$. This is a departure from the model discussed here and may be the result of the onset of collective depinning of vortices.[22,36] As in sample 1 (Fig. 3), the onset of nonlinearity in Fig. 5 for sample 2 also occurs at vortex displacements of only ~ 1 Å. The curves in Fig. 5 show the fits of Eq. (16) to the data. For this sample, we determine $\Delta R_{s0} = 4.7\times10^{-7}\Omega(\text{T GHz})^{-1}$ and $\Delta R_{s1} = 7.6\times10^{-7}\Omega(\text{T GHz K})^{-1}$ from the temperature dependence of the linear ΔR_s in the manner described in our discussion of Fig. 4. The free parameter for all of the $\Delta_H R_s$ fits is the product $r_P \times l$, which is the mean area of the vortex loop hopping between metastable states in response to the applied microwave current. For the fits shown in Fig. 5, the vortex loop area $r_P l$ was taken to be 12 nm^2. In these fits, we limited the range of U_δ by assuming $\nu(U_\delta)=0$ for $U_\delta > U_{\delta 0} = 2U_b$. However, this assumption only weakly affected the fits to the $\Delta_H R_s$ data. We have used the same $r_P l$, $U_{\delta 0}$, ΔR_{s0}, and ΔR_{s1} values for all three magnetic fields in Fig. 5 because, in the single-vortex limit, we expect the response of the vortices with respect to $I_{\rm rf}$ to be largely independent of magnetic field.

Figure 6 shows a plot of $\Delta_H R_s/f_n$ of sample 3 at 2 T and 5 K as a function of microwave current $I_{\rm rf}$ at 3 resonator frequencies: 1.69, 3.38, and 6.71 GHz. The inset to this figure shows the $\Delta_H R_s/f_n$ vs $I_{\rm rf}$ for the same frequencies and magnetic field but at 15 K. Because the curves in both the main figure and the inset are parallel and offset from each other by an amount proportional to the frequencies, these curves can be approximated as $\Delta_H R_s/f_n = a(I_{\rm rf}) + bf_n$ where the function $a(I_{\rm rf})$ arises from the current-driven hopping of vortices between metastable states for which $\Delta_H R_s \propto f$, and the second term arises from the linear motion of strongly pinned vortices for which $\Delta_H R_s \propto f_n^2$. Also shown on this figure are fits of Eq. (16) to these data based on the values of ΔR_{s0} and ΔR_{s1} obtained as described in our discussion of Fig. 4. For the fits to the $\Delta_H R_s$ data, the vortex loop area $r_P l$ is taken to be 26 nm^2. In order to fit the $\Delta_H R_s$ data in Fig. 7 we use $U_{\delta 0} = 2U_b + 40$ K which was determined through fits to the $\Delta_H X_s$. However this relation between $U_{\delta 0}$ and U_b

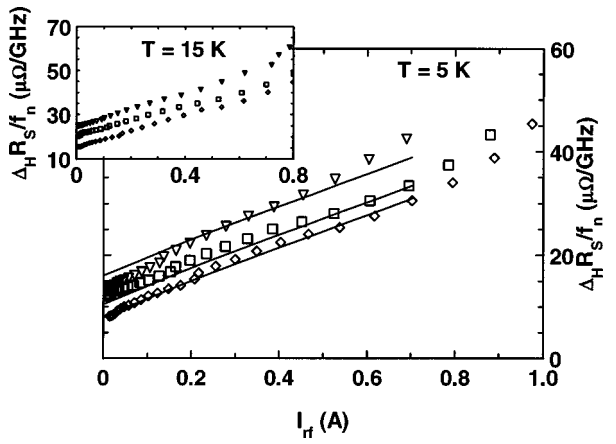

FIG. 6. The $\Delta_H R_s/f_n$ vs current $I_{\rm rf}$ for sample 3 at a temperature of 5 K and a magnetic field of 2 T for three frequencies: ($\diamond$) $f=1.69$ GHz, ($\square$) $f=3.38$ GHz, and ($\triangledown$) $f=6.71$ GHz. The curves show the fits of Eq. (16) to the data. The inset shows the $\Delta_H R_s/f_n$ vs $I_{\rm rf}$ data for sample 3 at a temperature of 15 K and a field of 2 T for the same three frequencies.

only weakly affects the fits to the $\Delta_H R_s$ data in Fig. 6. The onset of a linear $I_{\rm rf}$ dependence for $\Delta_H R_s/f_n$ is at a lower $I_{\rm rf}$ for sample 3 than in samples 1 and 2 which arises from the larger $r_P l$.[37] One of the most striking features of the data in Fig. 6 is the strong linear component to the $I_{\rm rf}$ dependence of $\Delta_H R_s/f_n$ which extends over a $\Delta_H R_s/f_n$ change of roughly 32 $\mu\Omega$/GHz. For the $f=1.69$ GHz data, this corresponds to a variation of $\approx 800\%$ as $I_{\rm rf}$ grows from 0 to 0.9 A. As in sample 1 (Fig. 3), the linear $I_{\rm rf}$ dependence of $\Delta_H R_s$ supports the assumption that the density of energy barriers between metastable vortex states $\nu(U_b)$ is roughly constant. As these data show, $R_s \sim f^1$ in the nonlinear limit. This arises because metastable segments are driven from $-r_P$ to r_P and back with each rf cycle. Since the energy loss in each transition is the same, $\Delta_H R_s$ arising from the proposed model is approximately proportional to frequency.

Figure 7 shows the changes in surface reactance $\Delta_H X_s$ of sample 3 as a function of resonator current $I_{\rm rf}$ at 5 K and 2 T for the frequencies 1.69, 3.38, and 6.71 GHz. Also shown in this figure (solid curves) are the $\Delta_H X_s$ predicted by Eq. (16), where we have used the same values of ΔR_{s0}, ΔR_{s1}, $r_P l$, and $U_{\delta 0}=2U_b+40$ K as those in Fig. 6 (see Table I). For the vortex-hopping loss mechanism, the increase in $\Delta_H X_s$, which is proportional to the number of vortices hopping between metastable states, has roughly the same magnitude as the increase in $\Delta_H R_s$. As discussed in Sec. III B, the $\Delta_H X_s \propto f^1$ frequency dependence of the fits arises because $\Delta_H X_s/f \sim E \propto \dot{u}$ multiplied by the number of metastable segments that can be polarized by $J_{\rm rf}$. For $J_{\rm rf}\phi_0 r_P l \gg k_B T$, this polarizability is largely frequency independent so that $\Delta_H X_s \propto \dot{u} \propto f$.

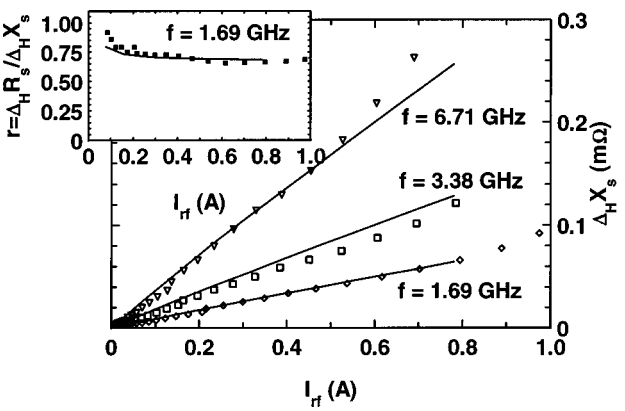

FIG. 7. The $\Delta_H X_s$ vs current $I_{\rm rf}$ (right scale) for sample 3 at a temperature of 5 K and a magnetic field of 2 T for three frequencies: ($\diamond$) $f=1.69$ GHz, ($\square$) $f=3.38$ GHz, and ($\triangledown$) $f=6.71$ GHz. The curves show the fits of Eq. (16) to the data. The inset shows $r=\Delta_H R_s/\Delta_H X_s$ vs $I_{\rm rf}$ for ($\blacksquare$) $f=1.69$ GHz.

The value $r=\Delta_H R_s(I_{\rm rf})/\Delta_H X_s(I_{\rm rf})$ is a parameter often used to differentiate between vortex loss mechanisms.[38,39] The inset to Fig. 7 shows a plot of r vs. $I_{\rm rf}$ taken from the surface resistance and surface reactance data plotted in Figs. 6 and 7.[40] These data and the results of the proposed model (solid line) both show an r value which decreases with increasing $I_{\rm rf}$. As others have shown,[38,39] r values near 1, such as those in this inset, are typical of hysteretic loss mechanisms.[12] The values of $r \sim 1$ for this type of loss mechanism arise because the motion of metastable vortex segments increases both the vortex lattice polarizability, which is the measure of $\Delta_H X_s$, and the vortex energy loss, which determines $\Delta_H R_s$. This is not generally true of other loss mechanisms. For instance, the r values are less than 10^{-2} for the nonlinearities due to the breaking of Cooper pairs into quasiparticles or to the nonlinear inductance of weak links, based on a quasiparticle relaxation time of $\approx 10^{-13}$ s,[38,41] while the current-induced heating of superconducting weak links is expected to generate r values of about 200.[38]

Figure 8 shows data for the $\Delta_H R_s$ and $\Delta_H X_s$ as a function of $I_{\rm rf}$ for sample 3 at temperatures 5, 10, and 15 K for a magnetic field of 2 T and a frequency of 1.69 GHz. Also shown in this figure is the fit of Eq. (16) to these data, in which we have used the values of R_{s0}, R_{s1}, and $r_P l$ previously determined for this sample (Table I) at each of the three temperatures.

In Fig. 8(a) the fits to $\Delta_H R_s$ are essentially straight lines with the same slope, offset from each other, which results from the assumption that $\nu(U_b)$ is roughly independent of U_b to energies of at least several hundred Kelvin. This implies that the number of pairs of metastable states within $k_B T$ of those with $U_b \approx J_{\rm rf}\phi_0 r_P l$ is independent of U_b. In the data, however, there is an increase in the separation of the three data sets as $I_{\rm rf}$ increases. At $I_{\rm rf}=0.7$ A, the separation between the surface resistance curves at the three temperatures has increased by roughly 35% or $4.4\times 10^{-6}\Omega$ above its value at $I_{\rm rf}=0.2$ A.This increasing separation could be incorporated into the fits to the data by causing $\nu(U_b)$ to increase slowly with U_b; however, the increase in separation could also arise from an increase in the loop area $r_P l$ with increasing $I_{\rm rf}$. As shown, however, the fits to the data are quite good without adjusting either $\nu(U_b)$ or $r_P l$.

Figure 8(b) shows the corresponding $\Delta_H X_s$ data and the fit of Eq. (16) to these data, with the same values of ΔR_{s0}, ΔR_{s1}, $U_{\delta 0}$, and $r_P l$ as Fig. 8(a) (see Table I). For large $I_{\rm rf}$, the $\Delta_H X_s$ of the 15 K data are roughly 7$\mu\Omega$ less than that of the 5 K data. However, the fits to these data suggest that the

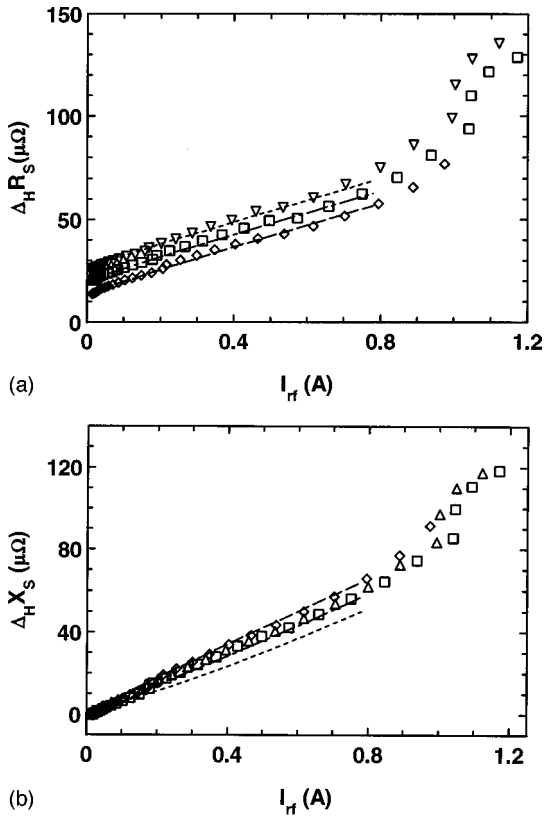

FIG. 8. (a) The $\Delta_H R_s$ vs current $I_{\rm rf}$ for sample 3 at a frequency of 1.69 GHz and a magnetic field of 2 T for three temperatures: ($\diamond$) $T=5.0$ K, ($\square$) $T=10.0$ K, and ($\triangledown$) $T=15.0$ K. The curves show the fits of Eq. (16) to the data. (b) $\Delta_H X_s$ vs $I_{\rm rf}$ for the three temperatures shown (a): ($\diamond$) $T=5.0$ K, ($\square$) $T=10.0$ K, and ($\triangle$) $T=15.0$ K with fits to Eq. (16).

surface reactance at 15 K should be roughly $17\mu\Omega$ less than that of the 5 K data at $I_{\rm rf}=0.7$ A. This discrepancy would be largely eliminated if the spreading of the $\Delta_H R_s$ data were incorporated into the fits in Fig. 8(a), and would result in a reduction in the separation of the $\Delta_H X_s$ fits in the inset to Fig. 8(b) by roughly $7\mu\Omega$.

In Figs. 8(a) and 8(b) the data at $I_{\rm rf}>1$A for the three temperatures and the separation between the data sets increase rapidly with increasing $I_{\rm rf}$. These increases probably indicate a more general depinning of the vortex lattice. For sample 3, a resonator current of $I_{\rm rf}=1$ A produces a $J_{\rm rf}\approx 3\times 10^7$ A/cm^2 on the edges of the resonator which corresponds to a mean vortex displacement on the edges of the resonator of $J_{\rm rf}\phi_0/\alpha_P\approx 30$ Å$\approx\xi$, roughly the pinning range of many types of defects. At this displacement a substantial number of vortices can be depinned. With a $r_P l$ of 26 nm^2, a current density of 3×10^7 A/cm^2 corresponds to a U_b of $\sim$1000 K.

V. COMPARISON WITH RELATED WORK

This is the first comprehensive work to characterize and explain the low-temperature dependence of ΔZ_s on $I_{\rm rf}$ in high-T_c films in the mixed state ($H\gg H_{c1}$) at microwave frequencies. We have shown previously in the linear regime at low microwave current that the frequency and temperature dependence of the dynamics of vortices can be explained by thermally activated hopping of vortices between pairs of metastable states separated by a uniform distribution of energy barriers.[8] In the present work we show that the same model which is able to explain the frequency and temperature dependence in the linear regime is readily employed to explain the nonlinear regime.

Our results show that at low temperatures the onset of nonlinearity is at $J_{\rm rf}\approx 2\times 10^6$ A/cm^2, which is comparable to the values given by other authors. For instance, Golosovsky *et al.*[12] also report a threshold value of 2.2×10^6 A/cm^2 at 5 K, and van der Beek *et al.*[22] report typical threshold values of 1.0×10^6 A/cm^2 at low temperatures. Though there is little previous experimental work to characterize the frequency and temperature dependence of the vortex-induced $\Delta_H Z_s$, there are a number of theories which have been proposed to address the nonlinear response of the vortex system; such theories generally assume a uniform vortex pinning potential. Van der Beek *et al.*[22] propose that the vortex pinning potential is sinusoidal in u_P, and that for large vortex displacements ($u>\xi\approx 20$ Å), the potential becomes nonparabolic, introducing nonlinearities. However, this model cannot explain the onset of nonlinearities at vortex displacements of ~ 1 Å$\ll\xi\approx 20$ Å.[7,38]

Other theories address the creation and destruction of vortices by the ac magnetic field.[32,42] However, in our measurements, the peak rf field is $\sim$1% of the dc magnetic field, so the variations in the vortex population arising from $I_{\rm rf}$ cannot account for the $\Delta_H R_s\sim 300\%$ variation we see in response to increases in $I_{\rm rf}$ (see Fig. 5).

In addition, there are theories which suggest that at sufficiently high vortex velocities, the vortex viscosity η will be reduced,[43,44] or increased.[45] At low temperatures, the theories that suggest that η will be reduced predict a reduction in $\Delta_H R_s$ with increasing $J_{\rm rf}$ for pinned vortices, contrary to what we find. The theories that predict an increasing η apply to vortex velocities greater than 2000 m/s. However, at 1 Å displacements and 1.23 GHz, our vortex velocities are only $\sim$1 m/s. So our vortex velocities are too small to test either of these theories.

Anderson and Kim[46] proposed that the effect of the current density would be to reduce the effective barrier heights for the hopping of vortices; however, they assumed a uniform periodic pinning potential that would lead to an $\Delta_H R_s\propto e^{-U_P/k_BT}\sinh J/J_c$ dependence. Our data show a roughly linear increase in $\Delta_H R_s$ with increasing $J_{\rm rf}$ contrary to the exponential increase in $\Delta_H R_s$ predicted by Anderson and Kim. Further, because this model assumes that the potential $U(u)$ is uniform, the effect of $J_{\rm rf}$ in lowering $U(u)$ would be to exponentially increase the population of thermally activated free vortices which, in the limit $\lambda_L\gg\rho/2\pi i\mu_0 f$, would give[8] $\Delta_H R_s\propto f^0$. Thus, Anderson and Kim's model would lead to a frequency-independent loss rather than the $\Delta_H R_s\propto f^1$ dependence exhibited in our data.

VI. DISCUSSION

The model proposed in this paper for nonlinear vortex dynamics assumes a strongly disordered pinning potential and vortices whose current-dependent hopping is dominated by pairs of metastable states. By quantitatively treating the effects of $J_{\rm rf}$ on the effective energy barrier heights between

metastable states, as well as by explicitly considering the probability distributions $\nu(U_b)$ and $\nu(U_\delta)$, our model for the high-frequency vortex dynamics reproduces the following features of the experimental data: the $\Delta_H R_s, \Delta_H X_s \propto I_{\rm rf}^1$ current dependence, the $\Delta R_s, \Delta X_s \propto f^1$ frequency dependence at all $I_{\rm rf}$, the $\Delta R_s \propto T^1$ temperature dependence at small $I_{\rm rf}$, and the $\Delta_H R_s \propto [a(I_{\rm rf})+T^1]f^1$ at large $I_{\rm rf}$, where $a(I_{\rm rf})$ is independent of temperature. Further, as we discuss below, the values of $r_P l$ and $U_{\delta 0}$ determined by the proposed model are consistent with the expectations of collective-pinning theory.

In order to understand the parameters r_p and l, we must consider the properties of vortices in high-T_c materials and the nature of their pinning. As others have shown,[3,47] the vortex pinning potential arises from the competition between two characteristic vortex energies: (1) the elastic energy for the deformation of the vortex lattice by vortex pinning sites, (2) the sample pinning potential resulting from the random distribution of defects.

Because of the small vortex core size in high-T_c materials, vortex cores are sensitive to the energy variations arising from point defects such as atomic vacancies or interstitials. Others have shown that the density of these defects in high-T_c materials is as high as 10 defects per core per layer in high-T_c materials.[3,47,48] The high density of metastable pinning sites that can explain the functional forms of our measured $\Delta Z_s(I_{\rm rf},T,f,H)$ we find in our results is consistent with their findings. Because of their small size, the potential $U(r) \approx -U_0 \exp[-3r^2/2\xi^2]$ arising from point defects[3,47] establishes a minimum length for $r_p \geq \xi \approx 20$ Å for our YBCO samples.

We put an upper bound on r_p and estimate the mean length l of a pinned vortex segment from the results of collective-pinning theory which shows that the elastic energies of the random deformation of the vortex lattice $U_{\rm el}$ are comparable to the energies of the pinning sites deforming the lattice. As a result, we find $U_{\rm el} \sim U_b, U_\delta$.[7,49,50]

In the low field single-vortex limit of collective-pinning theory,[3,50,51] the dominant elastic lattice energies $U_{\rm el}$ are tilting energies and arise from the motion of segments of vortex cores of length l with respect to the rest of that core. These energies are characterized by a tilt modulus:[7,51,52]

$$C_{44} \approx \frac{\sqrt{3} H \phi_0}{4\pi \Gamma \mu_0 \lambda_\parallel^2}, \tag{19}$$

where $\Gamma = \lambda_\perp / \lambda_\parallel \approx 5$ is an anisotropy factor. The energy of displacement U_t of a vortex segment of length l by a distance r_P is

$$U_t \approx C_{44} V_c (r_P/l)^2, \tag{20}$$

where V_c, the correlated volume of the vortex lattice, is the size of the lattice section within which all vortices are displaced by less than ξ from the locations that would correspond to a perfectly ordered lattice.[49] In the single-vortex limit, this volume V_c includes only one segment of length l and $V_c \approx a_0^2 l$, where $a_0 = (\phi_0/H)^{1/2}$. From Eq. (20) we see that as r_P increases the tilting energy for the vortex segment increases quickly particularly for small l. Thus U_t tends to limit r_P to $\sim \xi$. In order to determine an approximate value for l for strongly pinned vortex segments we equate U_t to the pinning energy for a vortex segment. From Eq. (9), the vortex restoring force per unit length α_P is determined by the curvature of the pinning potential. Since the range of the pinning potential is roughly r_P, the pinning energies $\sim U_t$ are estimated to be $\alpha_P l r_P^2/2$.[7,20] For the material parameters given in Table I we find that the l for pinned vortex segments ranges from $\sim \xi$ to ~ 100 Å. These small values for l suggest that the vortex lattice is strongly disordered and that the distribution of pinning energies will be very broad. For weakly pinned metastable vortex segments we expect l to be somewhat larger. However, since our measured $\Delta Z_s \propto H$ the vortices are in the single vortex limit and l for metastable vortex segments will be less then the vortex separation $a_0 \approx 300$ Å.[50]

From U_t, r_P, and l determined above, we can estimate the energies that characterize metastable vortex segments. Setting U_b, U_δ equal to U_t, and r_P to 20 Å we find $U_b, U_\delta \sim U_t(r_P, l)$ range from ~ 100 to ~ 5 K for $\xi < l < a_0$.

If we assume that the values for the horizontal displacements of the vortex loops r_P for our samples is about $\xi \approx 20$ Å, the dimensions of the vortex loops found through fits to the proposed model [Eq. (12)] are consistent with the predictions discussed above. For $r_P = 20$ Å in sample 2, we find from the $r_P l = 12$ nm^2 that the mean metastable segment length l is 60 Å. Similarly for sample 3, using the same r_P and $r_P l = 26$ nm^2, we obtain an l of 130 Å, and for sample 1 $l = 95$ Å. As discussed above, these lengths are consistent with the theories of collective pinning in the single vortex limit, which predict that a typical length of metastable segments l will be between ξ and the vortex lattice constant $a_0 = \sqrt{\phi_0/H} \approx 300$ Å for the field range studied above. Our determination of l is also in good agreement with the values determined from the onset of nonlinearity in these samples from which l is[7,35,50]

$$l \sim \xi \left(\frac{J_0}{J_c} \right)^{1/2}, \tag{21}$$

where $J_0 \approx 10^8$ A/cm^2 is the depairing current density. If we take J_c to be 1.8×10^6 A/cm^2 for sample 1 (Fig. 3), we obtain a value for l of 90 Å which agrees well with our experimental findings of $l \sim 95$ Å.

With the proposed model, we are able to fit the measured current, frequency, temperature, and field dependence of both $\Delta_H R_s$ and $\Delta_H X_s$ using two adjustable parameters per sample: the vortex loop area $r_P l$ which determines the rate of increase of $\Delta R_s(I_{\rm rf})$ with increasing $I_{\rm rf}$ and the shape of the distribution $\nu(U_\delta)$ which is determined by $U_{\delta 0}$. In fitting these data there are two issues that have yet to be resolved. The first is that the linear ΔR_s data have a $\propto f^{1.1}$ to $f^{1.4}$ frequency dependence,[7,8] while this model, using the approximations we have made, predicts a $\Delta R_s(f)$ proportional to $f^{1.0}$. The second is that, although the $\Delta_H R_s(T)$ data grow linearly with temperature as predicted by the model, the component of $\Delta_H R_s(T)$ which is $\propto f^1$ extrapolates to a small positive value in the limit of zero temperature (see Fig. 4). Both of these effects could result in part from a $\nu(U_b)$ which decreases with increasing U_b. However, we see no strong indication of such an effect in the $I_{\rm rf}$ dependence of our temperature-dependence data (see Fig. 8). It is more likely

that the deviations from a $\Delta R_s(f) \propto f^1$ frequency dependence arise from additional $\Delta R_s(f) \propto f^2$ viscous losses.

VII. CONCLUSION

We have presented measurements of the microwave surface impedance for YBCO thin films in the mixed state as a function of microwave current from the low-current, linear regime to the strongly nonlinear regime at $I_{rf} \sim 1$ A. Measurements were obtained in static magnetic fields of 1 to 4 T (well above $H_{c1} \approx 0.1$ T) as a function of frequency from 1.2 to 8.5 GHz at temperatures from 5 to 15 K. As this group[7,8] and others[12,13] have found, the results indicate that Z_s is roughly proportional to the dc magnetic field, indicating that we are studying the interactions between individual vortex cores and pinning sites in the YBCO films.

Previously we have shown[8] that in order to describe the linear response of vortices in high-T_c materials it is necessary to consider the thermally activated hopping of vortex segments between pairs of metastable vortex states. In the current work we have shown that this same model, first proposed by Koshelev and Vinokur at low frequencies and for T approaching T_c,[19] can be extended to explain the temperature, frequency, magnetic-field, and I_{rf} dependence of the nonlinear microwave Z_s in YBCO thin films if the barrier heights U_b between metastable vortex states in the linear-response model are replaced by effective barrier heights $\tilde{U}_b$ whose magnitudes are $U_b - J_{rf}(r,t) r_P l \phi_0$. By fitting our nonlinear response data to this model, we have found that the horizontal displacements of the vortex segments $r_P \approx \xi \approx 20$ Å and the lengths of those segments $l \approx 100$ Å, both of which are well within theoretical expectations.

ACKNOWLEDGMENTS

The work at MIT (AFOSR Agreement No. F49620-95-1-0027) and at Rome Laboratory (AFOSR Agreement No. F30602-95-2-0010) was supported by AFOSR. At the MIT Lincoln Laboratory, the work was supported by the Advanced Research Projects Agency (ARPA) under the auspices of the Consortium for Superconducting Electronics (CSE). We wish to thank R. P. Konieczka and D. Baker for help with device fabrication, G. Fitch for help with programming, and Dr. A. C. Anderson of MIT Lincoln Laboratory for supplying the high-T_c films, for many helpful discussions, and for critical reading of the manuscript.

*Present address: Bell Laboratories, Lucent Technologies, 600 Mountain Ave, Murray Hill, NJ 07974.

[1] G. D'Anna, W. Benoit, W. Sadowski, and E. Walker, Europhys. Lett. **20**, 167 (1992).
[2] Ph. Seng, R. Gross, U. Baier, M. Rupp, D. Koelle, R. P. Huebener, P. Schmitt, G. Saemann-Ischenko, and L. Schultz, Physica C **192**, 403 (1992).
[3] C. J. van der Beek and P. H. Kes, Phys. Rev. B **43**, 13 032 (1991).
[4] M. S. Pambianchi, D. H. Wu, L. Ganapathi, and S. M. Anlage, IEEE Trans. Appl. Supercond. **AS-3**, 2774 (1993).
[5] J. Owliaei, S. Sridhar, and J. Talvacchio, Phys. Rev. Lett. **69**, 3366 (1992).
[6] T. Schuster, H. Kuhn, E. H. Brandt, M. Indenbom, M. R. Koblischka, and M. Konczykowski, Phys. Rev. B **50**, 16 684 (1994).
[7] S. Revenaz, D. E. Oates, D. Labbe-Lavigne, G. Dresselhaus, and M. S. Dresselhaus, Phys. Rev. B **50**, 1178 (1994).
[8] N. Belk, D. E. Oates, D. A. Feld, G. Dresselhaus, and M. S. Dresselhaus, Phys. Rev. B **53**, 3459 (1996).
[9] D. E. Oates, A. C. Anderson, D. M. Sheen, and S. M. Ali, IEEE Trans. Microwave Theory Tech. **MTT-39**, 1522 (1991).
[10] D. M. Sheen, S. M. Ali, D. E. Oates, R. S. Withers, and J. A. Kong, IEEE Trans. Appl. Supercond. **AS-1**, 108 (1991).
[11] P. P. Nguyen, D. E. Oates, G. Dresselhaus, and M. S. Dresselhaus, Phys. Rev. B **48**, 6400 (1993).
[12] M. Golosovsky, M. Tsindlekht, H. Chayet, and D. Davidov, Phys. Rev. B **50**, 470 (1994).
[13] D. H. Wu and S. Sridhar, Phys. Rev. Lett. **65**, 2074 (1990).
[14] D. H. Wu, J. C Booth, and S. M. Anlage, Phys. Rev. Lett. **75**, 525 (1995).
[15] E. H. Brandt, Physica C **195**, 1 (1992).
[16] M. Daeumling, J. M. Seuntjens, and D. C. Larbalestier, Nature (London) **346**, 1332 (1990).
[17] E. V. Thuneberg, Cryogenics **29**, 236 (1989).
[18] J. I. Gittleman and R. Rosenblum, Phys. Rev. Lett. **16**, 734 (1966).
[19] A. E. Koshelev and V. M. Vinokur, Physica C **173**, 465 (1991).
[20] M. W. Coffey and J. R. Clem, Phys. Rev. Lett. **67**, 386 (1991).
[21] E. H. Brandt, Phys. Rev. Lett. **67**, 2219 (1991).
[22] C. J. van der Beek, V. B. Geshkenbein, and V. M. Vinokur, Phys. Rev. B **48**, 3393 (1993).
[23] A. S. Westerheim, L. S. Yu-Jahnes, and A. C. Anderson, IEEE Trans. Magn. **MAG-27**, 1001 (1991).
[24] A. S. Westerheim, A. C. Anderson, D. E. Oates, S. N. Basu, D. Bhatt, and M. J. Cima, J. Appl. Phys. **75**, 393 (1994).
[25] A. C. Anderson (unpublished).
[26] A. C. Anderson, D. E. Oates, R. L. Slattery, and L. S. Yu-Jahnes (unpublished).
[27] D. E. Oates, A. C. Anderson, C. C. Chin, J. S. Derov, G. Dresselhaus, and M. S. Dresselhaus, Phys. Rev. B **43**, 7655 (1991).
[28] Z.-D. Hao, J. R. Clem, M. W. McElfresh, L. Civale, A. P. Malozemoff, and F. Holtzberg, Phys. Rev. B **43**, 2844 (1990).
[29] N. C. Yeh, Phys. Rev. B **40**, 4566 (1989).
[30] N. C. Yeh and C. C. Tsuei, Phys. Rev. B **39**, 9708 (1989).
[31] M. W. Coffey and J. R. Clem, Phys. Rev. B **46**, 11 757 (1992).
[32] M. Golosovsky, M. Tsindlekht, and D. Davidov, Supercond. Sci. Technol. **40**, 1 (1996).
[33] G. Blatter, V. B. Geshkenbein, and V. M. Vinokur, Phys. Rev. Lett. **66**, 3297 (1991).
[34] In the linear J_{rf} limit discussed in our previous work (Ref. 8) the terms $\nu(U_\delta) \times T$ and $\nu(U_b)$ were absorbed into a single probability distribution $p(U_b)$, where $p(U_b)$ was the probability of finding two metastable states separated by an energy barrier U_b within $k_B T$ of each other. This approximation is valid in the limit of small J_{rf}, where it can be assumed that $\nu(U_\delta)$ is a constant.
[35] M. V. Feigel'man, V. B. Geshkenbein, A. I. Larkin, and S. Levit, JETP Lett. **57**, 711 (1993).
[36] V. M. Vinokur (private communication).
[37] Unfortunately the nature of the crossover from an I_{rf} independent to an I_{rf} dependent $\Delta R_s(I_{rf})$ is difficult to discern in this sample, because in the limit of small I_{rf}, this sample exhibits significant variations in $Z_s(I_{rf})$ both in field and at zero applied magnetic

field. The origin of these variations is however unclear, and they may arise from superconducting weak links near the edges of the resonator where the rf current density is strongly peaked.

[38] M. Golosovsky, M. Tsindlekht, H. Chayer, and D. Davidov, Phys. Rev. B **50**, 470 (1994); **51**, 12 062(E) (1995).

[39] J. Halbritter, J. Supercond. **8**, 691 (1995).

[40] In the inset to Fig. 7, we only plot r for $I_{rf}>0.08$ A, because, in the limit of low current, $\tilde{\Delta}X_s(I_{rf})=\Delta X_s(I_{rf})-\Delta X_s(0)$ is near 0 and small uncertainties in this quantity cause r to vary widely.

[41] K. Karrai, E. Choi, F. Dunmore, S. Liu, X. Ying, Q. Li, T. Venkatesan, H. D. Drew, and D. B. Fenner, Phys. Rev. Lett. **69**, 152 (1992).

[42] S. Sridhar, Appl. Phys. Lett. **65**, 1054 (1994).

[43] A. I. Larkin and Yu. N. Ovchinnikov, Zh. Eksp. Teor. Fiz. **68**, 1915 (1976).

[44] S. G. Doettinger, R. P. Huebener, R. Gerdemann, A. Kühle, S. Anders, T. G. Träuble, and J. C. Villégier, Phys. Rev. Lett. **73**, 1691 (1994).

[45] F. Guinea and Yu. Pogorelov, Phys. Rev. B **53**, 6725 (1996).

[46] P. W. Anderson and Y. B. Kim, Rev. Mod. Phys. **36**, 39 (1964).

[47] P. H. Kes and C. J. van der Beek, Physica B **169**, 80 (1991).

[48] P. H. Kes, Physica C **185-189**, 288 (1991).

[49] A. I. Larkin and Y. N. Ovchinnikov, J. Low Temp. Phys. **34**, 409 (1979).

[50] M. V. Feigel'man, V. B. Geshkenbein, A. I. Larkin, and V. M. Vinokur, Phys. Rev. Lett. **63**, 2303 (1989).

[51] V. M. Vinokur, P. H. Kes, and A. E. Koshelev, Physica C **168**, 29 (1990).

[52] A. Sudbø and E. H. Brandt, Phys. Rev. Lett. **66**, 1781 (1991).